RSC Advances

Dispersing Pt and Pd atoms on Au nanoparticles deposited on n-GaN substrates for formic acid oxidation

Journal:	*RSC Advances*
Manuscript ID	RA-COM-08-2015-016807.R1
Article Type:	Communication
Date Submitted by the Author:	14-Oct-2015
Complete List of Authors:	Qin, Shuang-jiao; Suzhou Institute of Nano-tech and Nano-bionics, Chinese Academy of Sciences, Zhao, Yu; Suzhou Institute of Nano-tech and Nano-bionics, Chinese Academy of Sciences, Peng, Fei; Suzhou Institute of Nano-tech and Nano-bionics, Chinese Academy of Sciences, Chen, Xue-Qing; Suzhou Institute of Nano-tech and Nano-bionics, Chinese Academy of Sciences, Pan, Ge-Bo; Suzhou Institute of Nano-tech and Nano-bionics, Chinese Academy of Sciences,
Subject area & keyword:	Electrocatalysis < Catalysis

Journal Name

COMMUNICATION

Received 00th January 20xx,
Accepted 00th January 20xx

DOI: 10.1039/x0xx00000x

www.rsc.org/

Dispersing Pt and Pd atoms on Au nanoparticles deposited on *n*-GaN substrates for formic acid oxidation

S.-J. Qin,[a,b] Y. Zhao,[b] F. Peng,[b] X.-Q. Chen,[b] and G.-B. Pan[b,*]

An ultimate low-loading Pt and Pd atoms on Au nanoparticles supported on *n*-GaN was prepared by electrochemical atomic layer deposition and surface-limited redox replacement. The asprepared electrocatalysts showed the enhanced performance for formic acid oxidation, and reached 3.5 mA μg_{PtPd}^{-1} in mass activity. The active sites of Pt^{Chem-O} species were found to play a key role in formic acid oxidation.

Proton exchange membrane fuel cells (PEMFC) are considered to be a promising technology for clean and efficient power generation.[1, 2] Direct formic acid fuel cells (DFAFC) are one of the most important types of PEMFC due to their high electromotive force, limited fuel crossover, and reasonable power density.[3-5] Pt and Pd are preferred anode catalyst for formic acid (FA) oxidation in acid media, however, they should be drastically optimized in both the anode and the cathode because their high costs.[6, 7] Meanwhile, they also have some shortcomings. Pd possesses high initial activity and produces less carbon monoxide (CO) for this reaction, but is much less stable.[8] Pt shows greater resistant to corrosion while readily poisoned CO by produced from dehydration of FA.[8, 9] It is generally agreed that the indirect oxidation pathway (dehydration of FA) requires continuous surface Pt lattices or dimer or trimer of Pt atoms.[10] The isolated Pt atom favours the direct oxidation pathway (dehydrogenation of FA) on its surface.[11] This has been proven using DFT calculations[12] and demonstrated by increasing coverage of Pt in the topmost mixed PtPd alloy layer could change the electrochemical formic oxidation mechanism from direct pathway to indirect pathway.[13]

Alloying Pt with Pd is one of promising solutions to accomplish a portion of goals in DFAFC and shows significantly higher stabilities and better activities than Pt or Pd alone.[14] Previous studies show that the oxidation of FA on both Pt and Pt–Ru is readily poisoned by adsorbed CO, while it is not greatly inhibited on Pt–Pd.[15] Theoretical work reveals that the d-band electronegativity or occupancy affects the adsorption energy of CO and H_2 on Pt sites.[16] On the other hand, greatest challenge is to reach 100% utilization of the catalytically active species while maintaining good enough durability against over oxidation and poisoning. Previous attempts have been made to grow monolayer-type Pt shell onto Pd cores with the enhanced mass catalytic activity toward the oxygen reduction reaction (ORR).[17, 18] Although, such structure could approach close the 100% Pt utilization, they are not favourable for formic acid oxidation because the continuous Pt atoms would facilitate the formation of poisoning CO intermediates *via* indirect pathway. Meanwhile, dispersing Pt atoms also have been deposited on conductive substrates through a molecular self-assembly/electro-deposition process and atomic layer deposition process.[11] It showed that single-atom catalysts exhibited superior electrocatalytic (up to 10 times) over that of commercial Pt/C catalyst due to the highly desired direct reaction path. Actually, alloying isolated Pt atoms with transition metals such as Pd atoms would be developed a better solution for optimizing performance and suppressing the indirect pathways.

Herein, we report a facile and one-cell configuration to form dispersed Pt atoms surrounded by Pd atoms onto Au nanoparticles (Au-PtPd NPs), which are electrodeposited on *n*-type gallium nitride (*n*-GaN). Our previous studies have shown that GaN might be a promising support for Pt, Au and Pd due to its high chemical stability, electric conductivity, and strong metal-semiconductor interaction.[19-21] The catalysts present the enhanced performance for FA oxidation, and their mass activity reaches 3.5 mA μg_{PtPd}^{-1}. The active sites of Pt^{Chem-O} species are the key roles for FA oxidation.

Electrochemical atomic layer deposition (E-ALD) and surface-limited redox replacement (SLRR) are a highly efficient route to grow atomic layer on gold substrates.[22-24] In a typical process, an atomic layer of sacrificial metal was formed by underpotential deposition (UPD) and subsequently replaced by

[a] Department of Chemistry, College of Sciences, Shanghai University, 99 Shangda Road, 200444 Shanghai, China.
[b] Suzhou Institute of Nano-tech and Nano-bionics, Chinese Academy of Sciences, 215123 Suzhou, China. Fax: +86 512 62872663, E–mail: gbpan2008@sinano.ac.cn
† Electronic Supplementary Information (ESI) available: Experimental detail in Fig. S1–S3. See DOI: 10.1039/c000000x/

noble metals in corresponding precursor ions. The redox replacement is limited by the coverage of UPD metals, and therefore monolayer films are produced. For instance, Pt and Pd monolayer can be deposited on single-crystal metallic electrodes of Au(111) and Rh(111).[25, 26] However, previously reports focus on depositing Pt or Pd monolayer for ORR, rather than the dispersing Pt and Pd atoms which presences discontinuous surface lattices and is more suitable for FA oxidation.

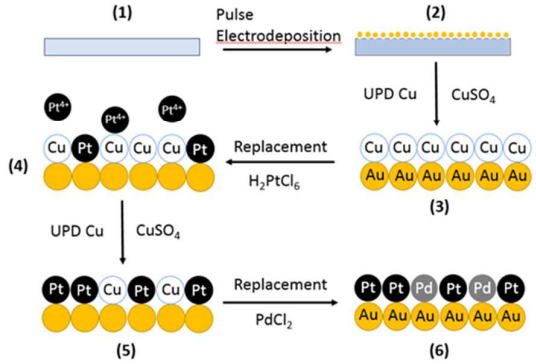

Fig. 1. Schematic illustration of the preparation of Au-PtPd on *n*-GaN(0001).

Fig. 1 shows a scheme of the preparation of Au-PtPd on GaN substrates. The Au NPs are prepared by pulse-current electrodeposition in 0.5 M NaCl + 1 mM $HAuCl_4$. The electrodeposition current densities are set at -20 mA cm^{-2} (1.5 s) and 0 mA cm^{-2} (4.5 s) (Fig. S1). The stabilized potential could be renewed after every pulse, indicating that the depletion zones would be repopulated with Au^{3+} during the time-off. Therefore, new nuclei are formed, rather than existing nuclei growth. Previous study had reported that ideal monolayer of Cu cannot be formed on Au NPs by a simple UPD, which was affected markedly by the deposition potential and time.[27] The Cu UPD is carried out at 0.2 V (before the OPD) for 10 s to form submonolayer absorbed Cu atoms in 0.1 M $NaClO_4$ + 10 mM $CuSO_4$ (Fig. S2). On the other hand, Cl^- adlayer on Au surface lattices such as c (2×2) structure would affect the Cu adatoms structure. When the presence of Cl^-, the (2×2) surface structure of Cu_{UPD}/Au(111) would transfer to (5×5) structure, and the interatomic spacing of Cu_{UPD} will increase to 3.67 Å.[28] Such route favours the formation of discontinuous surface lattices. Cu UPD adatoms were subsequently exchanged by Pt in 0.1 M $HClO_4$ + 0.4 mM H_2PtCl_6 at open circuit potential (Fig. S3). Pt coverage (θ_{Pt}) was calculated as the ratio of the charge from Cu adlayer oxidation. The calculated θ_{Pt} obtained *via* surface-limited redox replacement was approximately as 64% monolayer after two growth in this situation.[28] Then, the Cu UPD adatoms were re-deposited and exchanged in 0.1 M $HClO_4$ + 0.4 mM $PdCl_2$. With this method, the deposited Pt and Pd adatoms were fully exposed onto Au surface and formed the interactive Au-Pt, Au-Pd and Pt-Pd bonds. Moreover, Pd atoms embedded into Pt atom space, causing discontinuous surface Pt lattices and strengthen the self-stability. In comparison, the electrocatalysts of Pt or Pd monolayer on Au NPs (Au-Pt_{ML} or Au-Pd_{ML}) are deposited by similar routes.

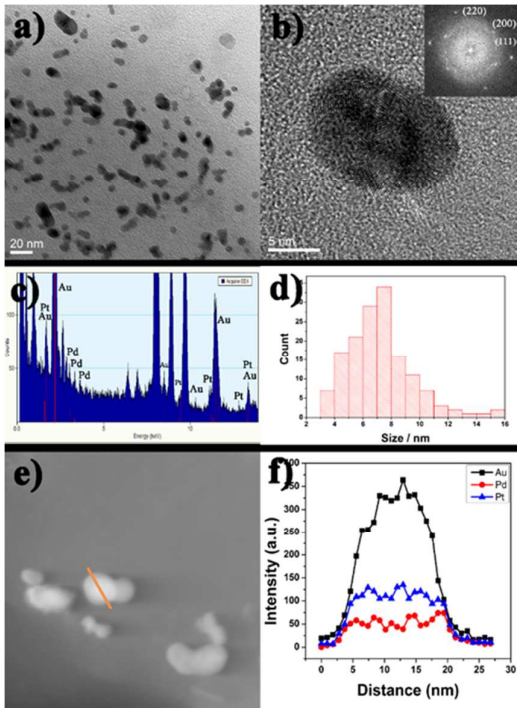

Fig. 2. The characterization of morphology and structure of Au-PtPd NPs, TEM (a), HR-TEM (b), EDS (c), size distribution (d), HR-STEM (e), and STEM-EDS (f).

The morphology and structure of the as-fabricated Au-PtPd NPs are investigated by transmission electron microscopy (TEM). Fig. 2a shows a typical TEM image, revealing sphere- or peanut-like NPs with the average diameter of ~7 nm. This is much smaller than those of NPs (~ 50 nm) grown by constant current electrodeposition and is due to a diffusion-limited nucleation. Fig. 2b shows a high resolution TEM (HR-TEM) image, and the inset is a corresponding faster Fourier transform (FFT) pattern. The bright diffraction spots are ascribed to the (220), (200) and (111) facets of Au, indicating polycrystalline nature of Au NPs. The lattice space of Au is clearly viewed, however, the structure of PtPd cluster could not be clearly certified due to ultimate low-loading. Fig. 2c shows energy-dispersive spectrum (EDS) for nanoparticles from a large area signal collection. Although the Pt and Pd content were too low to be determined quantitatively, their peaks present clearly in the spectrum with the relative low intensity. Furthermore, for single nanoparticle, the line profile analysis by STEM-EDS shows the distribution of Pt and Pd components (Fig. 2f). It is clear that Pt and Pd atoms fully cover around Au NPs. The identity of Pt and Pd components

along the centre of Au NPs is undulate slightly due to discontinuous surface distribution.

In addition to morphological characterization, the electrochemical properties of electrocatalysts are explored by cyclic voltammograms (CVs, Fig. 3a) in 0.5 M H_2SO_4 at a scan rate of 20 mV/s. Characteristic redox peaks (C_3/A_3) of Au at ~0.8 and 1.0 V disappear with the deposition of Pt and Pd atoms, and new redox peak appear at ~0.75 and 0.3 V. These are due to the loss of Au surface by masking with Pd and Pt atoms. Notably, with the cover of Pt and Pd atoms, the typical hydrogen adsorption/desorption in the negative and positive scans become sharper in the potential ranges from -0.3 to 0 V. The desorption peaks (A_2=-0.256 V and A_3=-0.201 V) ascribed to H desorption on Pt and Pd atoms with little negative shift are judged form Fig. S4. The enhanced peak current (C_4/A_4) at -0.09/-0.06 V attributed to H species in and out of lattice interstices of PtPd accompanied by H^+ electro-reduction and H electro-oxidation.[10] Meanwhile, electrochemically active surface area (ECSA) was calculated by the charges associated with H adsorption/desorption, assuming 210 mC cm^{-2} for oxidizing a monolayer of hydrogen on the catalyst. The ECSA of Au-PtPd NPs (100.15 m^2 g_{PtPd}^{-1}) is two times higher than commercial Pt/C catalyst and little higher than Pd@$Pt_{2\text{-}3L}$ octahedra nano-catalysts.[17] The stabilities of electro-catalyst was also evaluated by ECSA depended on prolonged CV tests in inset. The relative percentage of ECSA reduces to ~ 50% after 8000 cycles from -0.4 to 1.2 V. The more loss of ECSA for individual Pt_{ML} and Pd_{ML} on Au NPs are found after hundreds cycles. Noted that a clear relaxation phenomenon occurs at the initial 600 cycles, and then ECSA reduce rapidly to 75%, which reflects the weakness and instability of such catalysts in the initial stage of catalytic reaction. Similar phenomenon was also observed for 3% Pt@Au/C catalyst in the literature.[27] This is possibly because that the SLRR process only produce weakly adsorbed Pt and Pd atoms on Au NPs, i.e., do not form stable alloying. During the potential scan, surface atoms will rearrange into more stable structure. The catalysts display an activation stage in the initial scan. The active surface area is lost after 600 cycles, probably caused by the strong segregation of Pt/Au system or the dissolution of Pd.[27]

Fig. 3b shows CVs of Au-PtPd, Au-Pd_{ML}, and Au-Pt_{ML} NPs in 0.5 M H_2SO_4 + 0.2 M HCOOH at a scan rate of 50 mV/s. Compared with the Pt and Pd monolayer, the positive-scanning current shows a broad peak, consisted of two sub-peaks at around 0.1 and 0.3 V, which are the contribution of direct oxidation of FA to CO_2 on Pd and Pt atoms, respectively.[29] Although, the positive shift of oxidation peaks are 138 and 53 mV, respectively. In the negative scanning, the oxidation current increases until maximum current is obtained at about 0.02 V, which is attributed to the direct oxidation of FA on the restored Pd atoms. Meanwhile, the oxidation current is effectively inhibited in high potential range, indicating that indirect oxidation pathway is diminished. The presence of Au and Pd hinders CO formation on Pt atoms and shifts the oxidation onset potential to a much lower value. This is because Pd atoms block the aggregation of Pt atoms, single Pt atom surrounded by Pd atoms favour the direct oxidation of FA on these surfaces.[13] On the other hand, Au atoms also have a great influence on reaction pathways of Pt atoms. When the Pt:Au ratios less than 1:2 or θ_{Pt} less than 34 %, the indirect pathway become diminished.[30, 31] Simultaneously, Au-PtPd NPs has the enhanced catalytic performance, reached mass activity of 3.5 mA μg_{PtPd}^{-1} at 0 V. The inset shows the durability towards FA oxidation versus cycles. Half of the catalytic performance remains after 460 cycles, and similar relaxation phenomenon of increasing first and then decreasing has also been observed.

The oxidation states of Pt and Pd have been investigated by X-ray Photoelectron Spectroscopy (XPS). The Pt4f spectra exhibit a spin-orbit-split doublet, with two peaks ($4f_{7/2}$, $_{5/2}$) exhibiting a spacing of 3.3 eV. Before FA oxidation (Fig. 4a), two pairs of peaks, located at 71.22/74.52 and 72.19/75.49 eV, are assigned to Pt^0 and $Pt^{Chem\text{-}O}$, respectively.[29, 32] The $Pt^{Chem\text{-}O}$ surface core level shift shifts positively from 0.7 to 1.0 eV when

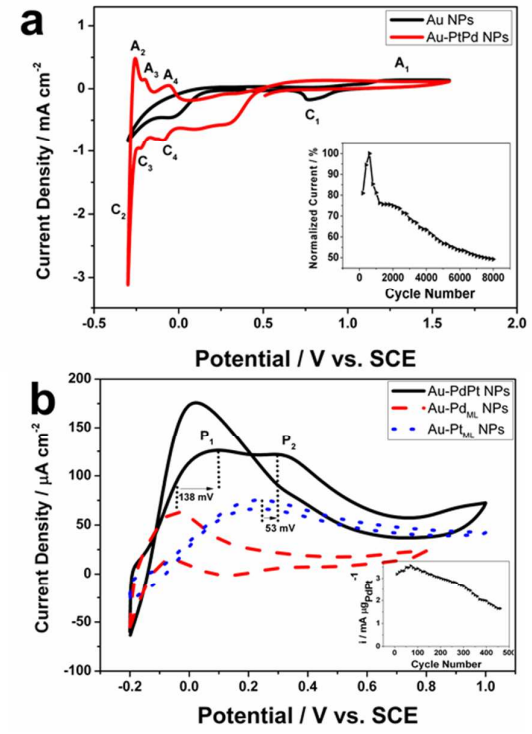

Fig. 3. CVs of Au, Au-Pt_{ML}, Au-Pd_{ML} and Au-PtPd NPs in 0.5 M H_2SO_4 at a scan rate of 20 mV/s (a), 0.5 M H_2SO_4 + 0.2 M HCOOH at a scan rate of 50 mV/s (b). The insets in (a) and (b) are the curves of ECSA and mass activity versus cycles, respectively.

GaN substrates used. Meanwhile, a very strong binding of oxygen to Pt atoms could be found. There still are 24.47 % of $Pt^{Chem\text{-}O}$ even in the fresh catalysts. It is mainly because that an

interfacial charge transfer process between the Pt and *n*-GaN substrates.[32] Noted that when subjected to FA oxidation (Fig. 4b), the relative percentage of Pt^{Chem-O} decrease to 13.06 %, the Pt^0 percentage increase 8.61 %, and Pt^{2+} (72.46 and 75.76 eV) is detected with the percentage of 2.8 %. Similarly, the Pd3d spectra (Fig. 4c) displays a doublet signal with binding energies of 335.3 and 340.6 eV for $3d_{5/2}$ and $3d_{3/2}$, respectively. After FA oxidation, another two small doublets (Fig. 4d) at 336.8 and 342.1 eV can be assigned to the Pd $3d_{5/2}$ and Pd $3d_{3/2}$ peaks of PdO species.[33] With the weaker oxygen absorption, Pd atoms present the entire zero value in the fresh catalysts, and after catalytic oxidation of FA the PdO species form with the percentage of 21.49 %.

The Pt^{Chem-O} species may play a role as active sites, resulting in the greatest decrement in composition. The chemisorbed oxygen on the Pt atoms presents a lower reaction barrier, intermediates are absorbed preferentially on Pt^{Chem-O} undergoing oxidation process to form CO_2 and the band of Pt-O fracture toward Pt^0 or Pt^{2+}. The kinetics of the CO oxidation reaction on Pt(111) surface preadsorbed p(2×2) layer of atomic oxygen had been investigated by HR-XPS.[34] The reaction of CO with preadsorbed O to CO_2 occurred on the top-sites or bridge-sites. The formation of Pt oxide state from chemisorbed oxygen has also been claimed on Pt single-crystal surface.[35, 36] Simultaneously, the interaction of Pd and Pt would give rise to some charge redistribution through hybridization of the states from each atom, so that the formation of PdOH prevails and PtOH is suppressed.[37] The final results are the formation of PdO species, and the percentage of Pt^0 increase. This corroborates the above proposition of the role of PdOH in suppressing a PtOH formation.

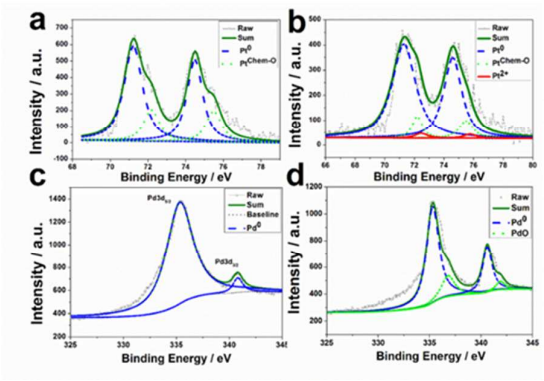

Fig. 4. XPS spectra of Pt4f (a, b) and Pd3d (c, d) before and after FA oxidation.

In summary, an ultimate low-loading Pt and Pd atoms on Au nanoparticles supported on *n*-GaN substrates are fabricated by electrochemical atomic layer deposition and surface-limited redox replacement, and presents enhanced electro-catalytic performance. The Pt^{Chem-O} species in such *n*-GaN-supported monolayer catalysts act as the active sites for formic acid oxidation, and the charge redistribution through hybridization of the states from Pt and Pd atoms could produce positive effect in the integral catalytic performance.

This work was financially supported by the National Natural Science Foundation of China (No. 21273272).

Notes and references

1 R. Taherian, *J Power Sources*, 2014, **265**, 370.
2 S. J. Peighambardoust, S. Rowshanzamir and M. Amjadi, *Int J Hydrogen Energ*, 2010, **35**, 9349.
3 X. W. Yu and P. G. Pickup, *J Power Sources*, 2008, **182**, 124.
4 U. B. Demirci, *J Power Sources*, 2007, **169**, 239.
5 K. J. Jeong, C. A. Miesse, J. H. Choi, J. Lee, J. Han, S. P. Yoon, S. W. Nam, T. H. Lim and T. G. Lee, *J Power Sources*, 2007, **168**, 119.
6 C. Rice, S. Ha, R. I. Masel and A. Wieckowski, *J Power Sources*, 2003, **115**, 229.
7 Z. L. Liu, L. Hong, M. P. Tham, T. H. Lim and H. X. Jiang, *J Power Sources*, 2006, **161**, 831.
8 C. X. Xu, Q. Hao and H. M. Duan, *J Mater Chem A*, 2014, **2**, 8875.
9 M. N. Cao, D. S. Wu and R. Cao, *Chemcatchem*, 2014, **6**, 26.
10 H. X. Zhang, C. Wang, J. Y. Wang, J. J. Zhai and W. B. Cai, *J Phys Chem C*, 2010, **114**, 6446.
11 R. Y. Wang, J. G. Liu, P. Liu, X. X. Bi, X. L. Yan, W. X. Wang, X. B. Ge, M. W. Chen and Y. Ding, *Chem Sci*, 2014, **5**, 403.
12 M. Neurock, M. Janik and A. Wieckowski, *Faraday Discuss*, 2008, **140**, 363.
13 C. H. Cui, H. H. Li, H. P. Cong, S. H. Yu and F. Tao, *Chem Commun*, 2012, **48**, 12062.
14 X. G. Li and I. M. Hsing, *Electrochim Acta*, 2006, **51**, 3477.
15 L. G. Feng, F. Z. Si, S. K. Yao, W. W. Cai, W. Xing and C. P. Liu, *Catal Commun*, 2011, **12**, 772.
16 E. Christoffersen, P. Liu, A. Ruban, H. L. Skriver and J. K. Norskov, *J Catal*, 2001, **199**, 123.
17 J. Park, L. Zhang, S. I. Choi, L. T. Roling, N. Lu, J. A. Herron, S. F. Xie, J. G. Wang, M. J. Kim, M. Mavrikakis and Y. N. Xia, *Acs Nano*, 2015, **9**, 2635.
18 X. Wang, S. I. Choi, L. T. Roling, M. Luo, C. Ma, L. Zhang, M. Chi, J. Liu, Z. Xie, J. A. Herron, M. Mavrikakis and Y. Xia, *Nature communications*, 2015, **6**, 7594.
19 Y. Zhao, S. J. Qin, Y. Li, F. X. Deng, Y. Q. Liu and G. B. Pan, *Electrochim Acta*, 2014, **145**, 148.
20 Y. Li, Y. Zhao, G. B. Pan, Z. H. Liu, G. L. Xu and K. Xu, *Electrochim Acta*, 2013, **114**, 352.
21 F. X. Deng, Y. Zhao, L. F. Hu, T. Xu, Y. Q. Liu and G. B. Pan, *Rsc Adv*, 2014, **4**, 42240.
22 N. Jayaraju, D. Vairavapandian, Y. G. Kim, D. Banga and J. L. Stickney, *J Electrochem Soc*, 2012, **159**, D616.
23 K. Sasaki, H. Naohara, Y. Cai, Y. M. Choi, P. Liu, M. B. Vukmirovic, J. X. Wang and R. R. Adzic, *Angew Chem Int Edit*, 2010, **49**, 8602.
24 R. R. Adzic, J. Zhang, K. Sasaki, M. B. Vukmirovic, M. Shao, J. X. Wang, A. U. Nilekar, M. Mavrikakis, J. A. Valerio and F. Uribe, *Top Catal*, 2007, **46**, 249.
25 Y. G. Kim, J. Y. Kim, D. Vairavapandian and J. L. Stickney, *J Phys Chem B*, 2006, **110**, 17998.
26 R. Hoyer, L. A. Kibler and D. M. Kolb, *Surf Sci*, 2004, **562**, 275.
27 Y. L. Yu, Y. P. Hu and X. Wang, *Electrochim acta*, 2009, **54**, 3092.
28 D. Gokcen, S. E. Bae and S. R. Brankovic, *J Electrochem Soc*, 2010, **157**, D582.

29 F. J. Vidal-Iglesias, J. Solla-Gullon, E. Herrero, A. Aldaz and J. M. Feliu, *Angew Chem Int Edit*, 2010, **49**, 6998.
30 N. Kristain, Y. L. Yu and X. Wang, *Electrochim acta*, 2009, **54**, 4916.
31 N. Kristain, Y. S. Yan and X. Wang, *Chem Comn*, 2008, 353.
32 S. Schafer, S. A. Wyrzgol, R. Caterino, A. Jentys, S. J. Schoell, M. Havecker, A. Knop-Gericke, J. A. Lercher, I. D. Sharp and M. Stutzmann, *J Am Chem Soc*, 2012, **134**, 12528.
33 M. Brun, A. Berthet and J. C. Bertolini, *J Electron Spectrosc*, 1999, **104**, 55.
34 M. Kinne, T. Fuhrmann, J. F. Zhu, C. M. Whelan, R. Denecke and H. P. Steinruck, *J Chem Phys*, 2004, **120**, 7113.
35 D. R. Butcher, M. E. Grass, Z. H. Zeng, F. Aksoy, H. Bluhm, W. X. Li, B. S. Mun, G. A. Somorjai and Z. Liu, *J Am Chem Soc*, 2011, **133**, 20319.
36 J. G. Wang, W. X. Li, M. Borg, J. Gustafson, A. Mikkelsen, T. M. Pedersen, E. Lundgren, J. Weissenrieder, J. Klikovits, M. Schmid, B. Hammer and J. N. Andersen, *Phys Rev Lett*, 2005, **95**.
37 J. Zhang, Y. Mo, M. B. Vukmirovic, R. Klie, K. Sasaki and R. R. Adzic, *J Phys Chem B*, 2004, **108**, 10955.

Graphical abstract

Dispersing Pt and Pd atoms on Au nanoparticles supported on *n*-GaN substrate was prepared. The catalysts present the enhanced performance for formic acid oxidation, and reached 3.5 mA μg_{PtPd}^{-1} in mass activity.